RSC Advances

ROYAL SOCIETY OF CHEMISTRY

www.rsc.org/advances

Synthesis and bioactivity of gelatin/multiwalled carbon nanotubes/hydroxyapatite nanofibrous scaffolds towards bone tissue engineering

Hualin Wang[a,b,*], Chengjiang Chu[a], Ruizhi Cai[a], Suwei Jiang[a], Linfeng Zhai[a], Jianfeng Lu[b,c], Xinjiang Li[b,c], Shaotong Jiang[b,c]

[a]*School of Chemistry and Chemical Technology, Hefei University of Technology, Hefei, Anhui 230009, People's Republic of China*

[b]*School of Biotechnology and Food Engineering, Hefei University of Technology, Hefei, Anhui 230009, People's Republic of China*

[c]*Anhui Institute of Agro-Products Intensive Processing Technology, Hefei, Anhui 230009, People's Republic of China*

Corresponding author: Hualin Wang, hlwang@hfut.edu.cn, Fax: 86-551-62901450, Tel: 86-551-62901450

ABSTRACT: The objective of this study was to develop a novel three-dimensional biomimetic gelatin/multiwalled carbon nanotubes/hydroxyapatite (gelatin/MWNTs/HA) nanofibrous scaffold *via* electrospinning technique for bone tissue engineering. The mechanical properties, structure, morphology and the bioactivity of nanofibrous scaffolds *in vitro* were investigated. Attentions were focused on the adhesion, mineralization, viability and proliferation of human fetal osteoblastic cells (hFOBs) on scaffold. Resulting scaffolds provided relative good mechanical support (7.9 ± 0.32 MPa) and high porosity (91.2%) to mimic a favorable environment for hFOBs. The hydrogen bonds between gelatin molecules and MWNTs/HA units were confirmed, and the incorporation of HA or MWNTs/HA nanoparticles caused an increase in porosity and strength of scaffolds, meanwhile the surface of nanofibers tended to be rough. HA nanoparticles showed a chelating effect to promote osteogenesis and mineralization of bone, and MWNTs had a synergetic effect with HA to induce the apatite formation. As compared to gelatin and gelatin /HA scaffolds, gelatin/MWNTs/HA scaffold exhibited the best viability hFOB cells cultured *in vitro*, most excellent morphology of hFOB cells seeded into scaffold and a significantly increasing in proliferation. The nanofibrous scaffold will have great potential as an excellent scaffold for in bone tissue engineering.

1. Introduction

For bone tissue engineering, a special subset of osteoinductive, osteoconductive, integrative and mechanically compatible materials is desirable[1,2]. Moreover, they need to provide an interface able to respond to local physiological and biological changes and to remodel the extracellular matrix (ECM) in order to integrate with the surrounding native tissue. Electrospun nanofibrous scaffolds have evinced tremendous attention to tissue engineering due to their three-dimensional porous structure similar to the fibrous architecture of the ECM[3-7].

Gelatin has been widely studied in tissue engineering because of its good affinity towards biological molecules and biological origin characteristic, as well as its formability and commercial availability at low cost[8,9]. However, gelatin has low mechanical properties due to the high degradation rate; when gelatin is crosslinked, high mechanical properties can be obtained[10,11]. Hydroxyapatite (HA) [Ca_{10} $(PO_4)_6(OH)_2$], the major inorganic component in human bone[12], is currently widely used as filler material for bone regeneration due to its similar chemical composition, crystallinity and morphology to the mineral constituents of human bones[13-15]. As an osteo-conductive and non-inflammatory biomaterial, HA can promote cell proliferation and osteoblastic cell differentiation[16,17]. Furthermore, the interaction between host bone and grafted biomaterial was enhanced by the chemical bonding from HA to natural bone [14,18].

These three-dimensional scaffolds should be mechanically strong to bear *in vitro* and *in vivo* stresses. It is an effective method to improve the mechanical strength by incorporating carbon nanotubes (CNTs) into the scaffolds[19]. Recently, CNTs have been drawn considerable attention to the applications in the field of tissue engineering due to their unique mechanical and chemical properties[20-23]: high-specific strength, excellent mechanical property, exceptional ability to functionalize bimolecular and the ability to be molded into various geometries and forms such as

porous structures, suitable for cell ingrowth, proliferation, and differentiation [24-26]. Multiwalled carbon nanotubes (MWNTs) have been confirmed good biocompatibilities with various cells, especially for osteoblast cells[27-30].

The aim of this work was to develop a novel biomimetic gelatin/MWNTs/HA nanofibrous scaffold *via* electrospinning technique for bone tissue engineering. To this aim, the mechanical properties, structure and morphology of scaffolds were characterized, and the bioactivity of scaffolds *in vitro* was assayed. The adhesion, mineralization, viability and proliferation of human fetal osteoblast (hFOBs) on these scaffolds were investigated emphasizely by morphology observation, cell counting, MTT and DAPI assay. For comparisons, gelatin and gelatin /HA scaffolds were electrospun.

2. Experimential

2.1 Materials

Porcine skin gelatin (G2500, type A) from Sigma (St Louis, MO, USA) was used without any treatment or further purification. Formic acid (98%) was obtained from Shanghai Lingfeng Chemical Reagent Co., Ltd. (Shanghai, China). Ammonium hydroxide solution (25-28%) was purchased from Shanxi Xinhua Chemical Reagent Co., Ltd. (Shanxi, China). Glutaraldehyde (biochemical reagent, 25%) was purchased from Sinopharm Group Chemical Reagents Co., Ltd. (Shanghai, China). All the chemical reagents used were of analytical grade. Multi-walled carbon nanotubes (MWNTs) (purity, 95%; diameter, 10-20 nm) were provided by Nanosolutions, Inc. (Jeonju, South Korea). The surfaces of the MWNTs were modified by attaching carboxylic acid functional groups through acid reflux treated (H_2SO_4/HNO_3, 3:1, v/v %)[31].

Human fetal osteoblastic cells (hFOBs) were obtained from the American Type Culture

Collection (ATCC, Arlington, VA, USA). Dulbecco's modified Eagle's medium/nutrient mixture F-12 (DMEM/F12) and fetal bovine serum(FBS) were purchased from GIBCO (Invitrogen Co., Carlsbad, CA, USA). Trypsin-EDTA was obtained from from Sigma (St Louis, MO, USA).

2.2. Preparation of samples

2.2.1 Electrospinning solutions

A gelatin electrospinning solution (50 wt%) was simply prepared by dissolving gelatin into 98 % formic acid under stirring at 50 ^{o}C for 2 h and then cooled naturally to ambient temperature. Assisted with stirring, 1 g calcium nitrate tetrahydrate was dissolved in distill water and the pH value of the solution was adjusted to 9 with ammonium hydroxide solution, and then a stoichiometric amount of ammonium dihydrogen phosphate solution (2 mol. L^{-1}) was added dropwise within 1 h. After stirring for 1 h, HA solution was obtained. To obtain gelatin/HA electrospinning solution, the required gelatin solution was mixed with HA solution and stirred about 0.5 h. Based on our experimental, the representative gelatin/HA electrospinning solution was chosen by the weight ratio of HA/gelatin at 4:6.

MWNTs with acid-treatment were added into above calcium nitrate tetrahydrate solution, and then stoichiometric amount of ammonium dihydrogen phosphate solution (2 mol. L^{-1}) was added dropwise to within 1 h and kept stirring for another 1 h. After filtered, the HA/MWNT composite nanoparticles were cleaned several times with deionized water until the pH of the suspension reached 7, and then washed with 1, 4-dioxane to remove the residue water. Assisted with stirring, the HA/MWNT nanoparticles were dispersed in 1, 4-dioxane again to form a suspension, and then required gelatin solution were added gradually into the suspension under at 50 °C till the weight ratio of HA/gelatin reached 4:6 to obtain gelatin/ HA/MWNT electrospinning solution.

2.3 Electrospinning procedures

The electrospinning device was consisted of a syringe, a needle (0.50 mm internal diameter), a coppersheet (10 cm × 10 cm × 0.1 mm), a ground electrode and a high-voltage power supply (DW-P403-1ACCC, Tianjin Dongwen, China). The supplied voltage was kept at 8 kV and the tip-to-collector distance (TCD) was kept at 12 cm. Electrospinning processing was carried out at room temperature. The result nanofibrous scaffolds were dried at 80 °C in vacuum condition for 24 h.

Gelatin, gelatin/HA and gelatin/MWNTs/HA scaffolds were crosslinked in 2.5 % glutaraldehyde solution at 4 ^{o}C for 24 hour, and the dried at 4 ^{o}C in an electrothermal constant-temperature drying oven. In order to investigate the interactions among gelatin, MWNTs and MWNTs, the scaffolds used in Fourier transform-infrared spectroscopy (FT-IR), X-ray diffraction (XRD) and Raman spectrum analysis were uncrosslinked. All the crosslinked scaffolds were used in the other tests.

2.4 Measurement and characterization

2.4.1 Mechanical characterization of nanofibrous scaffolds

For evaluating the influence of HA and HA/MWNT on the mechanical properties of the scaffolds, the tensile strength and elastic modulus of specimens were conducted on a TA-XTPlus Texture Analyser (Stable Micro Systems, Co., UK) using low force load cell of 10 N capacities. All the specimens were cut into rectangle (about 10 cm×2 cm×50 um). Dried films were conditioned at 50 % relative humidity (RH) and 25 ^{o}C for 48 h prior to mechanical testing. At least six samples were tested for each scaffold.

2.4.2 Porosity of nanofibrous scaffolds

The porosity of the scaffold was checked by bulk density method. In this method, the total porosity of the scaffold was calculated by following:

$$Porosity\ (\%) = 1 - \frac{\rho}{\rho_0} \times 100\% \quad (1)$$

where ρ is the bulk density of scaffold, ρ_0 is the true density of scaffold. True density was determined using Archimedes drainage method. During the calculation of bulk volume, the thickness of the scaffold was measured with a hand-held micrometer (BC Ames Co., Waltham, MA, USA). 15 measurements on different regions of on sample were performed, in order to obtain an accurate average value, and care was taken not deform the scaffold while measuring.

2.4.3 Morphology of nanofibrous scaffolds

The morphologies of nanofibrous scaffolds were examined by a field scanning electron microscopy (SEM) (Jeol JSM-6700F, Japan) and samples sputter-coated with gold at an accelerating voltage of 8 kV. SEM images were analyzed by Image Tool software, and a total of 50 counts were used to calculate the average diameter of nanofibres[32]. Transmission electron microscope (TEM) photograph was performed on an H-7650 microscopy (Hitachi, Japan) with an accelerating voltage of 220 kV.

2.4.4 Structure analysis

Fourier transform-infrared spectroscopy (FT-IR) study was completed with a Nicolet 6700 spectrometer (Thermo Nicolet, USA) in the range of 4000-400 cm^{-1} using a KBr pellet method. X-ray diffraction (XRD) analysis was measured with a D/max-γB rotating diffractomete (Rigaku, Japan), using CuKa (λ = 0.15418 nm). A scan rate of 0.05^o/s was applied to record the pattern in the 2θ range of $10\text{-}60^o$. Microscopic confocal laser Raman spectrometer was conducted with a LabRam HR Evolution (Paris, France) in the range of 1000-2000 cm^{-1}. A Raman spectrum

analysis (RM2000, Renishaw, U.K.; 632.8 nm, He-Ne Laser machines) was conducted to confirm the existence of MWNTs in the gelatin/MWNTs/HA nanofibrous scaffolds.

2.4.5 *In vitro* bioactivity of nanofibrous scaffolds

Gelatin, gelatin/HA and gelatin/MWNTs/HA scaffolds were immersed in a 1.5 × simulated body fluid (SBF) solution at 37 ^{o}C for 7 days in a constant-temperature incubator, every kind of scaffolds had three specimens. The initial pH value of the solution was set at 7.4 on the basis of the ion concentration of blood plasma. The composition of 1.5 × SBF was as follows: Na^{+}, 213.0 mM; K^{+}, 7.5 mM; Mg^{2+}, 2.25 mM; Ca^{2+}, 3.75 mM; Cl^{-}, 221.7 mM; HCO_3^{-}, 6.3 mM; HPO_4^{2-}, 1.5 mM; SO_4^{2-}, 0.75 mM. A surface area to volume ratio of 1.0 cm^{-1} was maintained for all immersions. The specimens were removed from the solution on the 7 th day, washed three times with distilled water to remove residue minerals, and then dried at low temperature (4 ^{o}C) in an electrothermal constant-temperature drying oven. The dried specimens were sputter-coated with gold (JEOL JFC-1600 Auto fine Coater, Japan) and examined by the SEM (Jeol JSM-6700F, Japan) in conjunction with energy dispersive X-ray spectroscopy (EDS).

2.4.6 hFOB cell culture

The hFOB cells were cultured in DMEM/F12 medium (1:1) containing 10% fetal bovine serum in 75 cm^2 flasks. The osteoblast culture was maintained in a humidified atmosphere of 5% CO_2 and 95% air at 37 ^{o}C and fed every three days. The hFOB cells were passaged with 0.25% trypsin/0.02% ethylenediamine tetraacetic acid (EDTA), then transferred to an osteogenic differentiation medium containing 80% DMEM/F12, 10% FBS and antibiotics (0.3 mg/ml G 418, 100 U/mL penicillin and 100 U/mL streptomycin sulfate). Populations of cell lines between passage 3 and 5 were used in the following tests.

2.4.7 Growth and mineralization of hFOB cell on nanofibrous scaffolds

Alizarin red-S staining was widely used to identify calcium in mineralization test[33,34]. An ARS-calcium complex was formed with calcium salts in a chelation process and the reaction was birefringent. Three kinds of scaffolds (crosslinked by with hFOB cells (constructs) after 7 days of culture were washed three times in PBS (pH 7.4) and dried in 70% ethanol for 1 h. After washed several times with deionized water, these constructs were stained with ARS (30 mM) for 20 min at room temperature. The stain was desorbed with 10% cetylpyridinium chloride for 1 h. The dye was collected and absorbance read at 540 nm in a spectrophotometer (Thermo Spectronic, USA).

2.4.8 hFOB cell proliferation assay

The hFOB cells were seeded (density: 3×10^4 cells/cm^2) on gelatin, gelatin/HA and gelatin/HA/MWNT nanofibrous scaffolds on 96 well plates. The cell responses to scaffolds were monitored by measuring the activity of the mitochondrial enzyme succinate dehydrogenase (SDH). After 1, 3, 5 and 7 days of cell culture, the cells were detached with 0.25% trypsin/0.02% EDTA at 37 ^{o}C for 10 min. Then an MTT (3-[4, 5-dimethyl-thiazol-2-yl-]-2, 5-diphenyl tetrazolium bromide) - succinate solution (20 μL, 0.5 mg/mL MTT) was added to each well and the plates were incubated again at 37 ^{o}C for 3 h. The cellular constructs were washed three times in PBS (pH 7.4) after MTT assay and the optical density (OD) of cellular constructs was read on an iMark™ Microplate Absorbance Reader (Bio-Rad, USA) at 490 nm. Every kind of scaffolds had five samples for MTT assay.

2.4.9 Processing hFOB cells for SEM

The hFOB cells were seeded (density: 3×10^4 cells/cm^2) on gelatin, gelatin/HA and

gelatin/HA/MWNT nanofibrous scaffolds on 96 well plates and cultured in an osteogenic differentiation medium. After 3 days culture, hFOB cells grown on scaffolds were washed with phosphate buffered saline (PBS, pH 7.4) to remove the non-adherent cells and then fixed in 3% glutaraldehyde for 3 h at room temperature, dehydrated by a series of graded alcohol solutions, treated with hexamethyl disilazan, and finally dried in air. Dried cellular constructs were sputtered with thick gold layer (JEOL JFC-1600 Auto fine Coater, Japan) and observed under the SEM (Jeol JSM-6700F, Japan) at an accelerating voltage of 10 kV.

2.4.10 hFOB cell morphology (DAPI)

The hFOBs were seeded (density: 3×10^4 cells/cm^2) on gelatin, gelatin/HA and gelatin/HA/MWNT nanofibrous and cultured in an osteogenic differentiation medium. After 7 days of culturing, the cellular constructs were rinsed with PBS (pH 7.4) and stained with 4', 6-diamidino-2-phenylindole (DAPI, Cell Tracker green, Promega USA) at a concentration of 10 μM. The cells were incubated 20 min at 37 ^{o}C with the dye, after incubation, the cells were rinsed with PBS (pH 7.4) and stained simultaneously by DAPI. hFOB morphology (excitation 360 nm, emission 440 nm) was observed using a Nikon Eclipse 80i fluorescence microscope (Nikon, Japan).

2.5 Statistical Analysis

Each experiment was repeated three times. Statistical analysis was performed using the unpaired Student's t-test, and the results were expressed as the means ± standard deviation (SD). A value of $p<0.05$ was considered to be statistically significant.

3. Results and discussion

3.1 Nanofibrous scaffold mechanical properties

The mechanical properties of scaffolds are important for the practical operations and applications in tissue engineering[35]. The stability of scaffolds to withstand stress is the necessity during culturing and implanting *in vitro*[36]. Mechanical properties of nanofibrous scaffolds were measured in terms of tensile strength and elastic modulus, and the results were summarized in Table 1. As could be seen from Table 1, the tensile strength of scaffold increases from 5.2 MPa (gelatin) to 6.3 MPa (gelatin/HA), meanwhile, the corresponding elastic modulus increases from

Table 1 Some properties of nanofibrous scaffolds: average fiber diameter, porosity, tensile strength and elastic modulus

Nanofibrousscaffold [a]	Average fiber diameter (nm)	Porosity (%)	Tensile strength (MPa)	Elastic modulus (MPa)
gelatin	200 ± 8.0	74.9 ± 2.6	5.2 ± 0.20	230 ± 9
gelatin/HA	160 ± 5.1	88.0 ± 4.1[#]	6.3 ± 0.26	368 ± 12[#]
gelatin/MWNTs/HA	180 ± 5.8	91.2 ± 4.4*,	7.9 ± 0.32*	820 ± 32*

[a] The data (mean ± SD) are results from three independent experiments.

[#] $p<0.05$, vs gelatin nanofibrous scaffold.

[*] $p<0.05$, vs gelatin/HA nanofibrous scaffold.

230 MPa to 368 MPa. When the matrix was subjected to stress, the rigidity HA nanoparticles initiated a mass of crazings that could consume a great deal of fracture energy, terminate and prevent them from further developing into flaws, thus improving the tensile strength. As expected, the incorporation of MWNTs/HA nanoparticles showed a further increase in tensile strength (7.9 MPa) and elastic modulus (820 MPa) as compared to gelatin/HA scaffold owing to the reinforcing effect of MWNTs. The obtained mechanical values for gelatin/MWNTs/HA scaffolds are adequate for bone tissue engineering. Kim *et al*[37] reported nanofiber generation of gelatin-hydroxyapatite biomimetics for guided tissue regeneration, the tensile strength and elastic modulus of gelatin-HA

scaffolds were at 4.6, 326 MPa (20% HA) and 4.4, 412 MPa (40% HA), respectively.

3.2 Nanofibrous scaffold morphology

A rough surface may provide abundant points for cell attachment and three-dimensional porous structure of scaffold will be favorable for nutrients and metabolic waste exchange[38,39]. Results on the SEM images of gelatin, gelatin/HA and gelatin/MWNTs/HA nanofibrous scaffolds were shown in Fig. 1 and the corresponding diameters of nanofibers are listed in Table. Fig. 1a showed the gelatin nanofibers with an average diameter about 200 nm were continuous and smooth on surface, while the average diameter of the gelatin/HA nanofibers decreased slightly to 160 nm, and the nanofibers were irregular in diameter and rough on surface(Fig. 1b). As compared to gelatin/HA nanofibers, the average diameter of gelatin/MWNTs/HA nanofibers increases to 180 nm (Fig. 1c) owing to the incorporation of MWNTs, meanwhile, the nanofibers tends to be more irregular in diameter and more beaded in morphology. As expected, the incorporation of HA or MWNTs/HA nanoparticles resulted in an increase in the porosity of the nanofibrous scaffolds (Table1): 74.9% (gelatin), 88.0% (gelatin/HA) and 91.2% (gelatin/MWNTs/HA), respectively. In general, the scaffolds with higher porosity are likely to support greater cellular proliferation and infiltration in tissue engineering[40,41].

TEM analysis was conducted to investigate MWNTs' structures and confirm the existence of MWNTs in the MWNTs/HA nanoparticles (Fig. 2). Fig. 2a showed the pristine MWNTs were smooth and entangled in bundles. After acid treatment, the pristine MWNTs degraded into shorter nanotubes without fullerenic caps and lots of defects were presented in the walls (Fig. 2b), which could work as active sites, meanwhile the carboxylic extremities of MWNTs could bind functional groups such as amines or hydroxyl groups. Fig. 2c was the high resolution TEM image of HA and

MWNTs matrix in MWNTs/HA nanoparticles. As shown in Fig. 2c, an interlayer spacing of the lattice of HA was 0.282 nm, corresponding to an interplanar distance of the (211) planes of HA observed from the XRD image (JCPDS No. 09-0432). Furthermore, an obvious characteristic lattice fringe of MWNTs was displayed and the distance between two fringes was 0.340 nm.

3.3 Nanofibrous scaffold microstructure

In this study, FT-IR analysis was used to determine the possible interactions between the components of scaffolds, and the FTIR spectra of the three nanofibrous scaffolds were shown in Fig. 3. In the FTIR spectrum of gelatin (Fig. 3a), peaks at 1654 cm^{-1} and 1541 cm^{-1} were attributed to stretching vibration of C=O for amide I and amide II, respectively, peak at 1239 cm^{-1} was associated with the stretching vibration of N-H. In the FTIR spectrum of MWNTs/HA (Fig. 3b), a strong characteristic absorption band at 3426 cm^{-1} was assigned to stretching vibration of –OH groups structured on HA and the corresponding deformation vibration absorption was at 633 cm^{-1}. Peaks at 1102 and 963 cm^{-1} were attributed to the stretching vibration of P–O bond in PO_4^{3-}, while peaks at about 603 and 566 cm^{-1} were associated with bending vibration of P–O bond in PO_4^{3-}. As could be seen from the FTIR spectrum of gelatin/MWNTs/HA (Fig. 3c), the stretching vibrations of C=O for amide I (1654 cm^{-1}) and amide II (1541 cm^{-1}), and that of N–H (1239 cm^{-1}) have shifted to lower wavenumbers at 1645, 1532 and 1229 cm^{-1}, respectively. Moreover, the characteristic absorption peaks of –OH (633 cm^{-1}) and PO_4^{3-} (963 cm^{-1}) for HA were disappeared, at the same time, the stretching vibration of –OH (3426 cm^{-1}) and PO_4^{3-} (1102 cm^{-1}) have shifted to lower wavenumbers at 3372 and 1095 cm^{-1}, respectively. These information implied that there existed hydrogen bonds of OH---OH or C=O---HO or N–H---P–O between gelatin molecules and MWNTs/HA units. Biocomposite nanofibrous scaffolds contain amino groups, carboxyl groups and

apatite to mimic the natural ECM for hFOB cells to attach, proliferate and migrate inside the nanofibrous scaffolds[42].

Fig. 4 illustrates the XRD patterns of gelatin, gelatin/HA and gelatin/MWNTs/HA scaffolds. As could be seen from Fig. 4a, gelatin showed a distinct broad peak at about $2\theta=20.25^{o}$. The pattern gelatin/HA (Fig. 4b) gave the principal diffraction peaks of HA at 2θ values of 25.98^{o} for reflection (002), at 28.43^{o} for reflection (102) and (210), at 31.9^{o} (triplet) for reflections (211), (112) and (300), and at 34^{o} for reflection (202), which could be identified according to JCPDS card No. 09-0432. It was noteworthy in Fig. 4c, a peak at for reflection (002*) of carbon was observed besides diffraction peaks of HA indicating the existence of the MWNTs (JCPDS card No.41-1487), which confirmed that MWNTs/HA nanoparticles had been incorporated into the matrix. Similar peak (002*) for carbon was reported in hydroxyapatite–carbon nanotube composite coatings[43].

The Raman spectra can confirm the presence of MWNTs in the gelatin/MWNTs/HA scaffold and also supply some detailed quantitative information about the microstructure of MWNTs[44,45]. As shown in Fig. 5a, Raman spectra for acid-treated MWNTs showed two characteristic peaks: one at 1340 cm^{-1} corresponding to the disorder-induced band (D band) and the other at 1570 cm^{-1} corresponding to the tangential mode (G band). The D mode reflected the disorder feature, whereas the G mode indicated the ordered graphite in the MWNTs. Furthermore, the area ratio of the intensity of the D band with respect to the G band (I_D/I_G) could be used as a measure of the disorder degree or the concentration of functionalized groups and defects and provide the quantitative information about the microstructure of MWCNTs. Higher I_D/I_G value revealed better graphitic structure in MWNTs, and the I_D/I_G of as-received MWNTs materials is was 0.80[46]. On the basis of Fig. 5a, the I_D/I_G of acid treated MWNTs was 0.97. This reflects that acid treatment could increase

the defects, modify the graphite structure and make MWNTs easily bonded with some chemical groups[47,48]. As compared to gelatin/HA scaffold (Fig. 5b), two unique apexes (D and G band) of MWNTs were found in the Raman spectra of gelatin/MWNTs/HA nanofibrous scaffold (Fig. 5c), implying the incorporation of MWNTs/HA nanoparticles into gelatin matrix.

3.4 *In vitro* bioactivity of nanofibrous scaffolds

As a preliminary investigation into the bioactivity, the prepared scaffolds were immersed in a 1.5 × SBF solution at 37 ^{o}C in a constant-temperature incubator. It could be clearly seen from Fig. 6 that minerals had been deposited on the surface of the scaffolds after 7 days of incubation, notably, the amount of minerals formed on the surfaces of scaffolds increased with this order: gelatin/MWNTs/HA > gelatin/HA > gelatin. This result might be due to the fact that the presence of HA and MWNTs nanoparticles in scaffolds decreased the surface energy for nucleation of minerals on the surface of the scaffolds. In addition, EDS results show that the crystalline areas formed on the surface of the gelatin/MWNTs/HA scaffold consist of Ca and P with a ratio Ca/P at 1.98 (average value of spectrum 1 and spectrum 2). In HA-containing scaffolds, HA nanoparticles could act as nucleation sites. First, Ca^{2+} deposited on HA nanoparticles owing to negative charge on their surface, then apatite could be formed more efficiently on the composite scaffolds than on gelatin scaffold[49]. As a result, more apatite was deposited on the HA-containing scaffolds than that on gelatin scaffolds in the same time interval. After acid treatment, MWNTs had negative charge on their surface[50], which favored the adsorption of Ca^{2+}, exhibiting a synergetic effect with HA to induce the formation of apatite. Once the apatite nuclei were formed, they were able to grow spontaneously by consuming the calcium and phosphate ions in the surrounding fluid. Therefore, the presence of HA and MWNTs enhanced the bioactivity of the scaffolds, which showed

excellent ability to undergo mineralization.

3.5 Growth and mineralization of hFOB cells on nanofibrous scaffolds

ARS staining was used to characterize the calcium minerals formation of hFOB cells cultured on scaffolds and the results on the quantitative analysis of the stain followed by their absorbance measurement were shown in Fig. 7. The absorbance values from Fig. 7 revealed a significant increase in calcium deposition on nanofibrous scaffolds by this order: gelatin/MWNTs/HA > gelatin/HA > gelatin. The porosity of scaffold is a critical feature affecting cell attachment, proliferation and migration, furthermore, surface topography is an another parameter that has been shown to affect the activity and biological function of cells[51]. As mentioned before, the incorporation of HA or MWNTs/HA nanoparticles resulted in an increase in the porosity and strength of scaffolds, meanwhile the surface of nanofibers tended to be rough. High porosity structure with comparative strength and rough surface was helpful to mimic the natural ECM and cells proliferation. On the other hand, HA nanoparticles could act as a chelating agent to promote osteogenesis and mineralization of bone, and MWNTs had a synergetic effect with HA to induce the apatite formation. As a result, osteoblast cells had grown better on the surface of gelatin/MWNTs/HA nanofibrous scaffolds, and then the amount of ECM secreted by cells for mineralization was greater than that of the other two groups.

3.6 Proliferation of hFOB cells on nanofibrous scaffolds

The viability of hFOB cells cultured on scaffolds was measured by an MTT cell proliferation assay, and the number of viable cells was assayed by cell counting under an inverted fluorescence microscope. The intrinsic mechanism of the MTT assay is that active cells react with a tetrazolium salt in the MTT reagent to produce a soluble formazan dye, which can be absorbed at a wavelength

of 490 nm[39]. As shown in Fig. 8, a consistent trend was presented in the cell counting and MTT assay results. The hFOB cell number was similar for the three tests, and no distinct differences in cell proliferation were observed on all the scaffolds at day 1. After 3 days of culturing, the gelatin/HA scaffold exhibited a slightly greater cell growth than that of gelatin scaffold ($p<0.05$). This was due to the fact that HA was biocompatible and could provide an effective site for cellular attachment. The hFOB cells on gelatin/MWNTs/HA scaffold showed greater growth than gelatin/HA scaffold ($p<0.05$), indicating that MWNTs might play an important role in cell adhesion and proliferation. The results after 5 and 7 days were similar to that of day 3. After 7 days of culturing, the number of hFOBs cells grown on gelatin/MWNTs/HA scaffold was almost 3 times than that of the initial seeding cells (30000 cells/cm^2), and 10 %, 60 % larger than that on the gelatin/HA ($p<0.05$) and gelatin scaffold ($p<0.05$), respectively, indicating that the viability and proliferation of hFOB cells were significantly promoted by growing on the gelatin/MWNTs/HA scaffold owing to the high porosity and relative rough surface. Mei *et al*[52] demonstrated that periodontalligament cells (PDLA) number on PLLA/MWNTs/HA nanofabrious membrane was almost almost 3 times than that of the initial seeding cells and 10 % larger than that on the PLLA/HA nanofabrious membrane for 7 days of culturing ($p<0.05$).

Figs. 9(a-c) show representative SEM morphologies of hFOB cells seeded into nanofibrous scaffolds after 3 days of culture. As observed in SEM, the hFOB cells on gelatin scaffold distributed sporadically (Fig. 9 a), whereas the hFOB cells on gelatin/HA and gelatin/MWNTs/HA scaffolds have been shown to develop a spindle shape with many filopodia extensions [Figs. 9 (b-c)]. In addition, hFOB cells grasped nanofibers tightly along the fibrous direction and some of them dispersed in internal scaffolds. The ECM secreted by cells was merged into the scaffolds and

crosslinked them tightly. Especially, the hFOB cells cultivated on gelatin/MWNTs/HA scaffold were flat and broad with large areas, and appeared more confluent, the corresponding cell density was superior to that of gelatin and gelatin/HA scaffolds after 3 days of culture, suggesting much better cell attachment and proliferation of gelatin/MWNTs/HA scaffold.

For the further investigation hFOB cell proliferation behavior on scaffolds, fluorescence microscope images were taken after 3 [Figs. 9 (e-f)] and 7 days [Figs. 9 (g-i)] of culture. The fluorescent images revealed better cellular viability and proliferation on gelatin/HA scaffold as compared to gelatin scaffold, this difference was amplified after 7 days of culture. The incorporation of HA particles into gelatin matrix increased the surface area and roughness of nanofibers which promoted the adhesion and proliferation of cells [Figs. 9 (e, h)]. Our results were in concordance with those of Deligianni et al[53], who also observed the incorporation of HA particles enhanced cell adhesion and proliferation of osteoblastic cells as the roughness increased. Furthermore, significant differences were found between gelatin/HA and gelatin/MWNTs/HA scaffolds, the higher hFOB cell proliferation was observed culturing on gelatin/MWNTs/HA scaffold after 7 days as compared to that on gelatin/HA nanofibrous scaffold. These results supported our MTT assay, where proliferation of cells on gelatin/MWNTs/HA scaffold was found to be better at day 7. It was demonstrated that gelatin/MWNTs/HA scaffold exhibited the best primary cell attachment characteristic and promoted higher cell viability and proliferation at the longer time interval of 7 days [Figs. 9 (f, i)], implying that the cell viability response was increased by MWNTs/HA nanopartcles for osteo-conductivity and bone-bonding ability in gelatin/MWNTs/HA scaffold. Mayer *et al*[54] demonstrated that biomaterials promoted higher cell activity or proliferation at the longer time interval of 10 days.

4. Conclusions

A novel three-dimensional biomimetic gelatin/MWNTs/HA nanofibrous scaffold was prepared *via* electrospinning technique, which was confirmed to be with good mechanical support, high porosity and wide range of pore size distribution to mimic a favorable environment for hFOB cells attachment, mineralization and proliferation. The interactions between gelatin molecules and MWNTs/HA units were proven to be hydrogen bonds. The incorporation of HA or MWNTs/HA nanoparticles resulted in an increase in porosity and strength of nanofibrous scaffolds, meanwhile the surface of nanofibers tended to be rough. HA nanoparticles could act as a chelating agent to promote osteogenesis and mineralization of bone, and MWNTs had a synergetic effect with HA to induce the formation of apatite. MTT and DAPI assay results showed that the best viability hFOB cells cultured *in vitro*, most excellent morphology of hFOB cells seeded into scaffold and a significantly increasing in proliferation as compared to gelatin and gelatin /HA scaffolds. In our opinion, the gelatin/MWNTs/HA nanofibrous scaffold will have great potential as an excellent scaffold for the soft bones such as nasal bone and ear bone in tissue engineering.

Acknowledgments

Financial support from National Natural Science Foundation of China (31171788) is gratefully acknowledged.

References

1. J.-H. Park, M.-K. Kim, A. El-Fiqi, S.-J. Seo, E.-J. Lee, J.-H. Kim and H.-W. Kim, *RSC Adv*., 2014, **4**, 29062.
2. S. Kumar, S. Bose and K. Chatterjee, *RSC Adv*., 2014, **4**, 19086.
3. N. Bhardwaj and S.C. Kundu, *Biotechnol. Adv.*, 2010, **28**, 325.
4. J.M. Holzwarth and P.X. Ma, *Biomaterials*, 2011, **32**, 9622.
5. S. Zhong, Y. Zhang and C.T. Lim, *Tissue Eng. Part B Rev*., 2011, **18**, 77.
6. Y.Z. Cai, G.R. Zhang, L.L. Wang, Y.Z. Jiang, H.W. Ouyang and X.H. Zou, *J. Biomed. Mater. Res. Part A*, 2012, **100**, 1187.

7. R. Sahay, P. S. Kumar, R. Sridhar, J. Sundaramurthy, J. Venugopal, S. G. Mhaisalkar and S. Ramakrishna, *J. Mater. Chem.*, 2012, **22**, 12953.
8. N. Mhd Sarbon, F. Badii and N.K. Howell, *Food Hydrocolloids*, 2013, **30**, 143.
9. A. Lu, J. Zhu, G. Zhang and G. Sun, *J. Mater. Chem.*, 2011, **21**, 18674.
10. X. Liu, L.A. Smith, J. Hu and P.X. Ma, *Biomaterials*, 2009, **30**, 2252.
11. M. Kharaziha, M. Nikkhah, S.-R. Shin, N. Annabi, N. Masoumi, A.K. Gaharwar, G. Camci-Unal and A. Khademhosseini, *Biomaterials*, 2013**, 34**, 6355.
12. J. Chen, Q. Yu, G. Zhang, S. Yang, J. Wu and Q. Zhang, *Colloid Surface B-Biointerfaces,* 2012, **93**, 100.
13. I. Armentano, M. Dottori, E. Fortunati, S. Mattioli and J. Kenny, *Polym. Degrad. Stabil*., 2010, **95**, 2126.
14. H. Zhou and J. Lee, *Acta. Biomater*., 2011, **7**, 2769.
15. A. Kolk, J. Handschel, W. Drescher, D. Rothamel, F. Kloss, M. Blessmann, M. Heiland, K.-D. Wolff and R. Smeets, *J. Cranio. Maxill. Surg*., 2012, **40**, 706.
16. J R. Jayakumar, K.P. Chennazhi, S. Srinivasan, S.V. Nair, T. Furuike and H. Tamura, *Int. J. Mol. Sci*., 2011, **12**, 1876.
17. M. Ohno, K. Kimoto, T. Toyoda, K. Kawata and H. Arakawa, *J. Oral. Implantol*., 2013, **39**, 154.
18. A. Jaiswal, H. Chhabra, V. Soni and J. Bellare, *Mater. Sci. Eng. C-Mater. Biol. Appl*., 2013, **33**, 2376.
19. M. Ayatollahi, S. Shadlou, M. Shokrieh and M. Chitsazzadeh, *Polym. Test .,* 2011, **30**, 548.
20. F. Liang and B. Chen, *Curr. Med. Chem*., 2010, **17**, 10.
21. E. Heister, E.W. Brunner, G.R. Dieckmann, I. Jurewicz and A.B. Dalton, *ACS Appl. Mater. Inter*., 2013, **5**, 1870.
22. P. Newman, A. Minett, R. Ellis-Behnke and H. Zreiqat, *Nanomedicine: Nanotechnol. Biol. Med.*, 2013, **9**, 1139.
23. E. Murugan and S. Arumugam, *RSC Adv*., 2014, **4**, 35428.
24. G.A. Snook, P. Kao and A.S. Best, *J. Power Sources*, 2011, **196**, 1.
25. L. Zheng, Z. Li, S. Bourdo, K.R. Khedir, M.P. Asar, C.C. Ryerson and A.S. Biris, *Langmuir*, 2011, **27**, 9936.
26. F.M. Tonelli, A.K. Santos, K.N. Gomes, E. Lorencon, S. Guatimosim, L.O. Ladeira and R.R. Resende, *Int. J. Nanomed.*, 2012, 7, 4511.
27. C. Lin, Y. Wang, Y. Lai, W. Yang, F. Jiao, H. Zhang, S. Ye and Q. Zhang, *Colloid Surface B-Biointerfaces*, 2011, **83**, 367.
28. Z. Song, Z. Yang, J. Yang, Z. Liu, Z. Peng, R. Tang and Y. Gu, *PloS one*, 2013, **8**, e64358.
29. L. Chen, J. Hu, X. Shen and H. Tong, *J. Mater. Sci. Mater. Med.* 2013, **24**, 1843.
30. H. Zhang and Z. Chen, *J. Bioact. Compat. Polym.* 2010, **25**, 241.
31. C. Su, L. Xu, R.-J. Yan, M.-Q. Chen and C. Zhan, *Mater. Chem. Phys.* 2012, **133**, 1034.
32. D.Z. Yang, Y.N. Li and J. Nie, *Carbohyd. Polym.* 2007, **69**, 538.
33. Y. Zhang, J.R. Venugopal, A. El-Turki, S. Ramakrishna, B. Su and C.T. Lim, *Biomaterials*, 2008, **29**, 4314.
34. S.-W. Tsai, H.-M. Liou, C.-J. Lin, K.-L. Kuo, Y.-S. Hung, R.-C. Weng and F.-Y. Hsu, *PloS one*, 2012, **7**, e31200.
35. H. Tan, J. Wu, L. Lao and C. Gao, *Acta Biomater* ., 2009, **5**, 328.
36. J. Fan, Y. Shang, Y. Yuan and J. Yang, *J. Mater. Sci. Mater. Med.*, 2010, **21**, 319.

37. H.W. Kim, J.H. Song and H.E. Kim, *Adv. Funct. Mater.*, 2005, **15**, 1988.

38. R. Ravichandran, C.C. Ng, S. Liao, D. Pliszka, M. Raghunath, S. Ramakrishna and C.K. Chan, *Biomed. Mater.*, 2012, **7**, 015001.

39. J. Venugopal, P. Vadgama, T.S. Kumar and S. Ramakrishna, *Nanotechnology*, 2007, **18**, 055101.

40. J. Zeltinger, J.K. Sherwood, D.A. Graham, R. Müeller and L.G. Griffith, *Tissue Eng.*, 2001, **7**, 557.

41. K. Rezwan, Q. Chen, J. Blaker and A.R. Boccaccini, *Biomaterials*, 2006, **27**, 3413.

42. J. Venugopal, S. Low, A.T. Choon, T.S. Kumar and S. Ramakrishna, *J. Mater. Sci. Mater. Med.*, 2008, **19**, 2039.

43. B.-D. Hahn, J.-M. Lee, D.-S. Park, J.-J. Choi, J. Ryu, W.-H. Yoon, B.-K. Lee, D.-S. Shin and H.-E. Kim, *Acta biomater.*, 2009, **5**, 3205.

44. T. McNally, P. Pötschke, P. Halley, M. Murphy, D. Martin, S.E. Bell, G.P. Brennan, D. Bein, P. Lemoine and J.P. Quinn, *Polymer*, 2005, **46**, 8222.

45. M. Evora, D. Klosterman, K. Lafdi, L. Li and L. Silva, *Radiat. Phys. Chem.*, 2013, **84**, 105.

46. K. Yang, M. Gu, Y. Guo, X. Pan and G. Mu, *Carbon*, 2009, **47**, 1723.

47. L.D. Tijing, W. Choi, Z. Jiang, A. Amarjargal, C.-H. Park, H.R. Pant, I.-T. Im and C.S. Kim, *Curr. Appl. Phys.*, 2013, **13**, 1247.

48. S.J. Aravind and S. Ramaprabhu, *ACS Appl. Mater. Inter.*, 2012, **4**, 3805.

49. S. Liao, G. Xu, W. Wang, F. Watari, F. Cui, S. Ramakrishna and C.K. Chan, *Acta Biomater.*, 2007, **3**, 669.

50. L. Zhao, H. Liu and N. Hu, *Anal. Bioanal. Chem.*, 2006, **384**, 414.

51. Q.P. Pham, U. Sharma and A.G. Mikos, *Biomacromolecules*, 2006, **7**, 2796.

52. F. Mei, J. Zhong, X. Yang, X. Ouyang, S. Zhang, X. Hu, Q. Ma, J. Lu, S. Ryu and X. Deng, *Biomacromolecules*, 2007, **8**, 3729.

53. D.D. Deligianni, N.D. Katsala, P.G. Koutsoukos and Y.F. Missirlis, *Biomaterials*, 2000, **22**, 8.

54. U. Meyer, D. Szulczewski, K. Moller, H. Heide, D. Jones, U. Gross, P. Vanwachem, F. Bagamdisa, A. Dekker and J. Davies, *Cells Mater.*, 1993, **3**, 129.

Figure captions

Fig. 1. SEM images of nanofibrous scaffolds: (a) gelatin, (b) gelatin/HA, (c) gelatin/MWNTs/HA.

Fig. 2. TEM images of samples: (a) pristine MWNTs, (b) acid treatment MWNTs, (c) high resolution TEM image of HA and MWNTs matrix in MWNTs/HA nanoparticles.

Fig. 3. FTIR spectra of samples: (a) gelatin scaffold, (b) MWNTs/HA nanoparticles, (c) gelatin/MWNTs/HAscaffold.

Fig. 4. XRD pattern of nanofibrous scaffolds: (a) gelatin, (b) gelatin/HA, (c) gelatin/MWNTs/HA.

Fig. 5. Raman spectra of samples: (a) acid treatment MWNTs, (b) gelatin/HA scaffold, (c) gelatin/MWNTs/HA scaffold.

Fig. 6. SEM images of nanofibrous scaffolds (in 1.5×SBF, 37 ^{o}C): (a) gelatin, (b) gelatin/HA, (c) gelatin/MWNTs/HA; (d) magnification for c, ×4; (e) and (f): the corresponding EDS spectra from (d).

Fig. 7. Quantification of mineral deposition in hFOB cells by ARS staining on nanofibrous scaffolds. The data (mean±SD) are results from three independent experiments. In the graph the p values are reported with respected to gelatin scaffold ($^{\#}p<0.05$) and gelatin scaffold (*$p<0.05$).

Fig. 8. hFOB cells proliferation on nanofibrous scaffolds: (a) cell counting , (b) MTT assay. The data (mean±SD) are results from three independent experiments. In the graph the p values are reported with respected to gelatin scaffold ($^{\#}p<0.05$) and gelatin scaffold (*$p<0.05$).

Fig. 9. SEM and fluorescence microscope images of hFOB cells attached on nanofibrous scaffolds. SEM micrographs: (a) gelatin, (b) gelatin/HA and (c) gelatin/HA/MWNTs after 7 days of culture, respectively; fluorescence microscope images: (d, g), (e, h) and (f, i) after 3 and 7 days of culture, respectively. Nucleus (blue) were stained with DAPI) are shown.

Figures

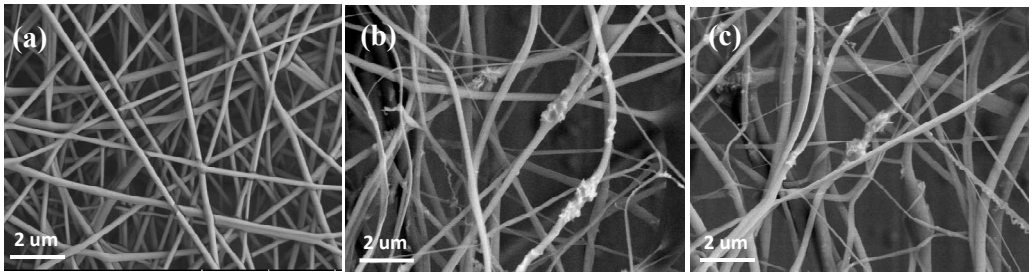

Fig. 1. SEM images of nanofibrous scaffolds: (a) gelatin, (b) gelatin/HA, (c) gelatin/MWNTs/HA.

Figures

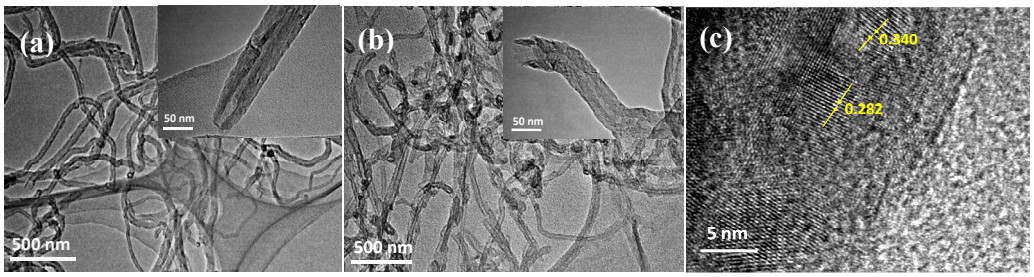

Fig. 2. TEM images of samples: (a) pristine MWNTs, (b) acid treatment MWNTs, (c) high.

Figures

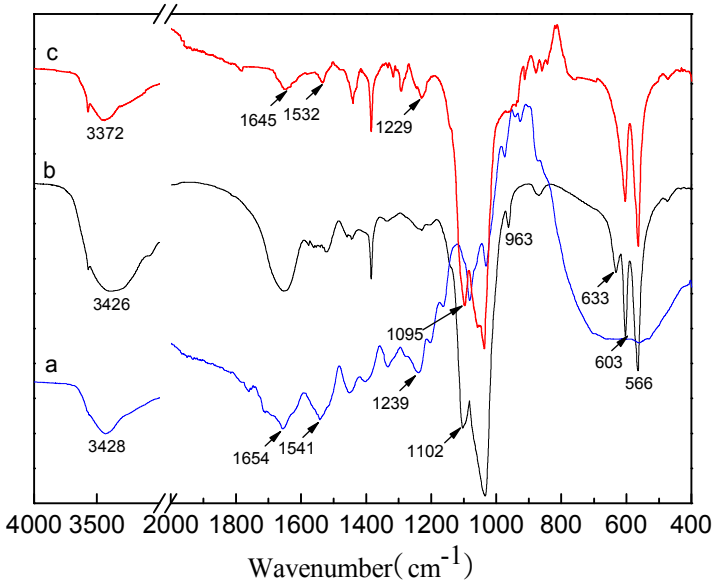

Fig. 3. FTIR spectra of samples: (a) gelatin scaffold, (b) MWNTs/HA nanoparticles, (c) gelatin/MWNTs/HAscaffold.

Figures

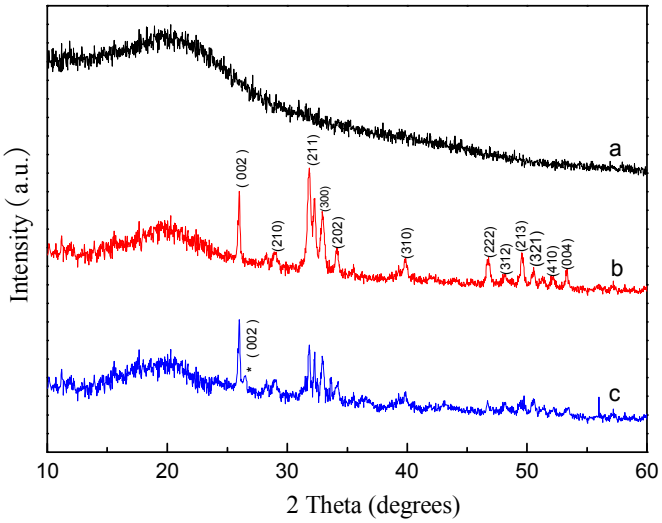

Fig. 4. XRD pattern of nanofibrous scaffolds: (a) gelatin, (b) gelatin/HA, (c) gelatin/MWNTs/HA.

Figures

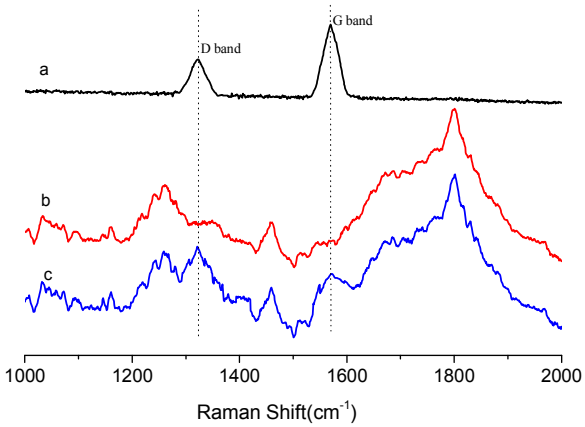

Fig. 5. Raman spectra of samples: (a) acid treatment MWNTs, (b) gelatin/HA scaffold, (c) gelatin/MWNTs/HA scaffold.

Figures

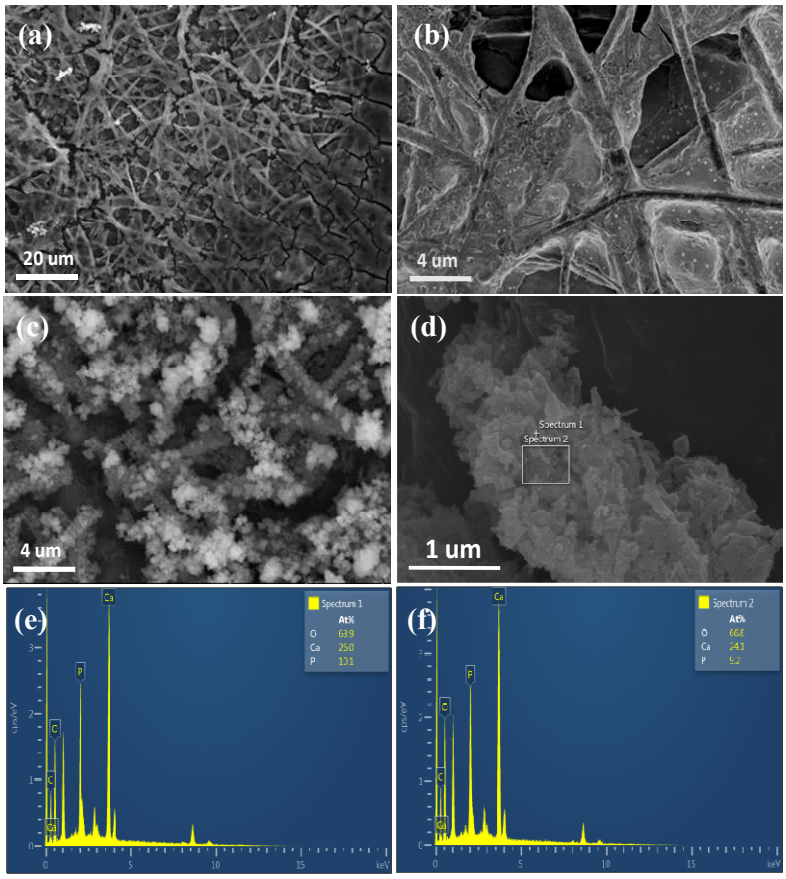

Fig. 6. SEM images of nanofibrous scaffolds (in 1.5×SBF, 37 ^{o}C): (a) gelatin, (b) gelatin/HA, (c) gelatin/MWNTs/HA; (d) magnification for c, ×4; (e) and (f): the corresponding EDS spectra from (d).

Figures

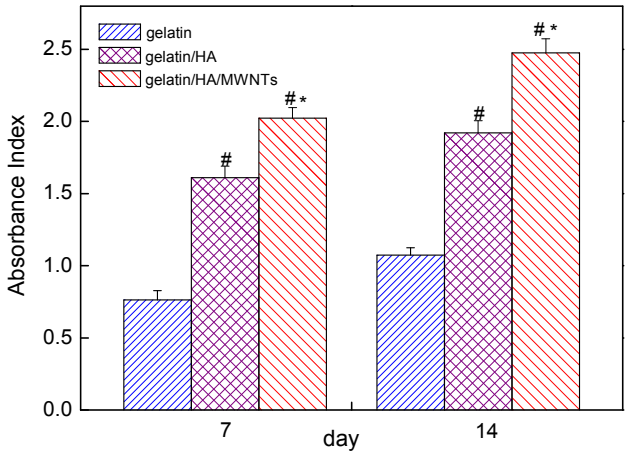

Fig. 7. Quantification of mineral deposition in hFOB cells by ARS staining on nanofibrous scaffolds. The data (mean ± SD) are results from three independent experiments. In the graph the p values are reported with respected to gelatin scaffold ($^{\#}p<0.05$) and gelatin scaffold ($^{*}p<0.05$).

Figures

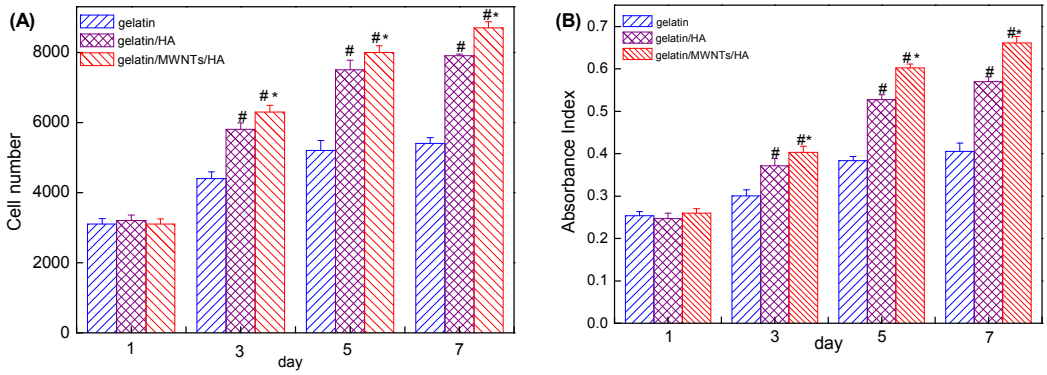

Fig. 8. hFOB cells proliferation on nanofibrous scaffolds: (a) cell counting , (b) MTT assay. The data (mean±SD) are results from three independent experiments. The data (mean±SD) are results from three independent experiments. In the graph the p values are reported with respected to gelatin scaffold ($^{\#}p<0.05$) and gelatin scaffold ($^{*}p<0.05$).

Figures

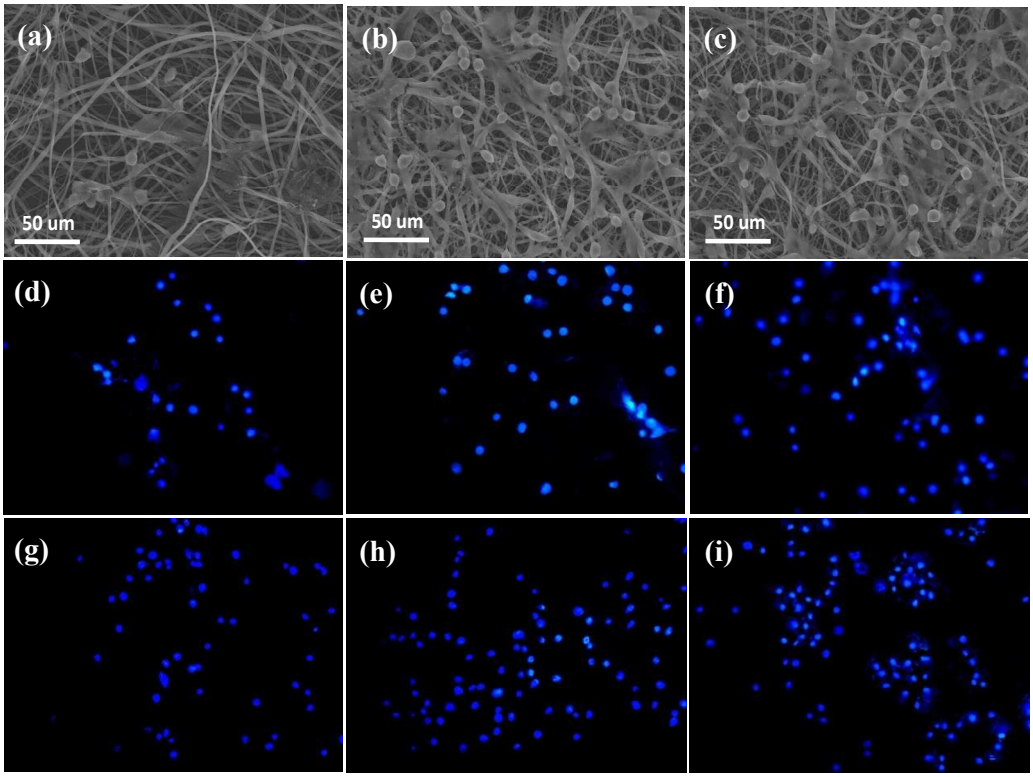

Fig. 9. SEM and fluorescence microscope images of hFOB cells attached on nanofibrous scaffolds. SEM micrographs: (a) gelatin, (b) gelatin/HA and (c) gelatin/HA/MWNTs after 7 days of culture, respectively; fluorescence microscope images: (d, g), (e, h) and (f, i) after 3 and 7 days of culture, respectively. Nucleus (blue) were stained with DAPI) are shown.

Table of contents entry

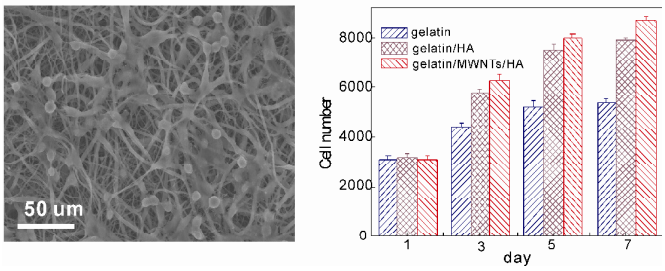

The *in vitro* bioactivity of scaffolds, and the adhesion, mineralization, viability and proliferation of hFOBs on Gelatin/MWNTs/HA nanofabrious scaffolds